



## Reliable individual differences in fine-grained cortical functional architecture

Ma Feilong<sup>a</sup>, Samuel A. Nastase<sup>a,b</sup>, J. Swaroop Guntupalli<sup>a,c</sup>, James V. Haxby<sup>a,\*</sup>

<sup>a</sup> Department of Psychological and Brain Sciences, Dartmouth College, Hanover, NH, USA

<sup>b</sup> Princeton Neuroscience Institute, Princeton University, Princeton, NJ, USA

<sup>c</sup> Vicarious AI, Union City, CA, USA



### ARTICLE INFO

#### Keywords:

fMRI  
Functional alignment  
Hyperalignment  
Individual differences  
Natural vision  
Reliability

### ABSTRACT

Fine-grained functional organization of cortex is not well-conserved across individuals. As a result, individual differences in cortical functional architecture are confounded by topographic idiosyncrasies—i.e., differences in functional–anatomical correspondence. In this study, we used hyperalignment to align information encoded in topographically variable patterns to study individual differences in fine-grained cortical functional architecture in a common representational space. We characterized the structure of individual differences using three common functional indices, and assessed the reliability of this structure across independent samples of data in a natural vision paradigm. Hyperalignment markedly improved the reliability of individual differences across all three indices by resolving topographic idiosyncrasies and accommodating information encoded in spatially fine-grained response patterns. Our results demonstrate that substantial individual differences in cortical functional architecture exist at fine spatial scales, but are inaccessible with anatomical normalization alone.

### 1. Introduction

Functional architecture of the human brain is relatively consistent across individuals at a coarse scale, but idiosyncrasies in functional topography become increasingly apparent at finer scales. Large-scale brain systems can be reliably identified across individuals by functional connectivity (Power et al., 2011; Yeo et al., 2011), but there is profound interindividual variability in system details (Gordon et al., 2017a, 2017b). At the areal level, category-selective regions can be localized to anatomical landmarks (Weiner et al., 2018, 2014), though the locus can differ across individuals by millimeters or centimeters, along with variability in size and shape (Zhen et al., 2017, 2015). Furthermore, within a brain area, between-subject classification of response patterns is typically considerably worse than within-subject classification (e.g., Cox and Savoy, 2003; Haxby et al., 2011), indicating that fine-grained functional architecture is not well-aligned macroanatomically. With state-of-the-art cortical surface-based alignment (Fischl, 2012), the mismatch between brain function and anatomy can be reduced but not eliminated (Duncan et al., 2009; Frost and Goebel, 2012; Weiner et al., 2018). Therefore, it is problematic to assume that a given anatomical location or topographic conformation will have the same functional role across brains. Individual differences in

neural function are confounded by individual differences in functional–anatomical correspondence.

Hyperalignment (Guntupalli et al., 2016, 2018; Haxby et al., 2011) is a family of methods that can disentangle functional variability from anatomical variability. Hyperalignment projects features (voxels or surface vertices) from a brain into a common high-dimensional space through linear transformations. In this common space, the same features from different individuals will share similar functional properties instead of the same anatomical locations or topographic conformations. Hyperalignment decomposes the original fMRI data of each individual into two parts: a transformation matrix, which reflects topographic properties of the individual's functional activations; and a new data matrix in the common space, which reflects shared, stimulus-driven responses. This hyperaligned data matrix provides an opportunity to study brain functions without confounds from topographic variability.

Besides separating interindividual variability in brain function from that in functional topography, hyperalignment also makes efficient use of functional neuroimaging data by utilizing spatially fine-grained pattern information. For example, between-subject classification improves severalfold by using hyperalignment instead of anatomical alignment (Guntupalli et al., 2018, 2016; Haxby et al., 2011). Coarse-scale

\* Corresponding author.

E-mail address: [james.v.haxby@dartmouth.edu](mailto:james.v.haxby@dartmouth.edu) (J.V. Haxby).

<https://doi.org/10.1016/j.neuroimage.2018.08.029>

Received 9 April 2018; Received in revised form 10 August 2018; Accepted 13 August 2018

Available online 15 August 2018

1053-8119/© 2018 The Authors. Published by Elsevier Inc. This is an open access article under the CC BY-NC-ND license (<http://creativecommons.org/licenses/by-nc-nd/4.0/>).

information, such as category selectivity or retinotopy, is encoded in a spatially smooth and similar fashion across neighboring voxels in a brain region. By contrast, fine-scale information, such as within-category distinctions among exemplars, is encoded in spatial patterns comprising different responses across voxels within a region. Fine-grained topographies exist across all of cortex (Guntupalli et al., 2018, 2016; Haxby et al., 2014, 2011), and encode fine-scale information (e.g., Haxby et al., 2001; Kriegeskorte et al., 2008) and details of interactions between brain regions (Guntupalli et al., 2018; Visconti di Oleggio Castello et al., 2017) that are not captured by coarse-scale responses such as the average response of a brain region. Importantly, individual differences in cognitive function may be expressed in differences in the fine-scale functional topographies that carry fine-scale information (Charest et al., 2014). Because anatomical alignment does not capture the shared information that is encoded in fine-scale topographies, individual differences in anatomically-aligned data multiplexes misalignment of functional architecture with individual differences in function. Consequently, the spatial granularity of individual differences in functional architecture that can be accessed with anatomically-aligned data may not match the spatial scale of the functional architecture that carries cognitive differences. Many researchers opt to sacrifice fine-grained information to boost coarse-grained information through spatial smoothing or averaging (Carp, 2012), making fine-grained information inaccessible to further analysis.

Recent advances have increased the utility of fMRI for studying the neural bases of individual differences (Dubois and Adolphs, 2016). Functional responses and connectivity measured by fMRI can predict an individual's intelligence (Heuvel et al., 2009; Smith et al., 2013), creativity (Beatty et al., 2018), personality (Adelstein et al., 2011; DeYoung et al., 2010), and can facilitate diagnosis (Arbabshirani et al., 2017; Wolfers et al., 2015) and prognosis (Gabrieli et al., 2015) of psychiatric disorders. However, it is still common practice to use feature sets derived by averaging voxels within a region or a network (Wolfers et al., 2015), thereby focusing only on individual differences in coarse-scale functional architecture. Given that fine-scale functional architecture has the potential to reveal individual differences in perception, cognition, and mental representation (Charest et al., 2014), it is critical to assess whether the information encoded in fine-grained functional architecture, when properly aligned across individuals, can be efficiently utilized for individualized predictions. In the current study we focused on the reliability of individual differences in the information encoded in cortical functional architecture. Establishing a correlational relationship between two measures, such as individual differences in cortical functional architecture and individual differences in behavior, is limited by the reliability of each measure, which reflects relative signal-to-noise. The highest possible correlation between two measures is constrained by their reliabilities, known as “attenuation by errors” (Spearman, 1904). Therefore, the reliability of individual differences in functional architecture quantifies the potential to predict other individual differences.

In this study, we used hyperalignment to examine individual differences in cortical functional architecture in a common representational space. Critically, this common space resolves idiosyncrasies in functional–anatomical correspondence. We indexed cortical functional architecture based on response profiles, functional connectivity, and representational geometry, and assessed the reliability of individual differences across independent samples of data using a natural vision paradigm. We found that with hyperaligned data, individual differences in cortical functional architecture were more reliable, and this increased reliability results primarily from the incorporation of fine-scale cortical functional architecture into our model. Our results suggest that substantial individual differences exist at a fine spatial scale, but are obscured by idiosyncratic functional–anatomical correspondence; hyperalignment can reveal these fine-scale individual differences, and make observed individual differences in cortical functional architecture more reliable.

## 2. Materials and methods

### 2.1. Participants

Twenty healthy young adults (mean age  $\pm$  standard deviation:  $24.4 \pm 3.4$  years, 12 females) participated in this study. All participants were right-handed, with normal hearing and normal or corrected-to-normal vision, and no known history of neurological illness. They gave written, informed consent, and were paid for their participation. The study was approved by the Institutional Review Board of Dartmouth College.

### 2.2. Stimuli and design

Participants watched a full-length audiovisual movie, *Raiders of the Lost Ark*, while fMRI data were collected. The movie was divided into eight parts, each 14–15 min in duration. Participants viewed four parts of the movie in each of the two scanning sessions, and were taken out of the scanner between the two sessions for a break.

The video was projected from an LCD projector onto a rear projection screen, and then reflected through a mirror on the head coil. The corresponding visual angles subtended approximately  $22.7^\circ$  horizontally and  $17^\circ$  vertically. The audio was played through MR-compatible headphones (MR confon GmbH, Magdeburg, Germany). Participants were instructed to pay attention to the movie and enjoy.

### 2.3. MRI acquisition

MR images were acquired using a 3T Philips Intera Achieva scanner with a 32-channel head coil at the Dartmouth Brain Imaging Center.

Functional images comprised  $80 \times 80 \times 42$  3 mm isotropic voxels, providing whole brain coverage. They were acquired every 2.5 s with an echo planar imaging (EPI) sequence (TR = 2.5 s, TE = 35 ms, flip angle =  $90^\circ$ ,  $80 \times 80$  matrix, FOV =  $240 \text{ mm} \times 240 \text{ mm}$ , SENSE reduction factor = 2, 42 interleaved axial slices). The length of a run was adjusted to match the length of the corresponding movie part, consisting of 326–344 vol each. In total, we acquired 2718 functional images per participant during 8 runs of movie watching (approximately 2 h of functional data per participant).

A high resolution T1-weighted image ( $0.9375 \text{ mm} \times 0.9375 \text{ mm} \times 1.0 \text{ mm}$  voxel resolution) was also acquired in each session with an MPRAGE sequence (TR = 8.2 ms, TE = 3.7 ms, flip angle =  $8^\circ$ ,  $256 \times 256$  matrix, FOV =  $240 \text{ mm} \times 240 \text{ mm}$ , 220 axial slices), except for one session of one participant.

### 2.4. MRI preprocessing

MRI data were first preprocessed using the fMRIPrep software version 1.0.0-rc2 (Esteban et al., 2018; <https://github.com/poldracklab/fmriprep>). T1-weighted images were corrected for bias field (Tustison et al., 2010) and skullstripped using `antsBrainExtraction.sh`. High resolution cortical surfaces were reconstructed with FreeSurfer (Fischl, 2012; <http://surfer.nmr.mgh.harvard.edu/>) using all available anatomical images, and registered to the fsaverage template (Fischl et al., 1999). Functional data were motion corrected using MCFLIRT (Jenkinson et al., 2002), and resampled to the fsaverage template based on boundary-based registration (Greve and Fischl, 2009). After these steps, functional data from all participants were in alignment with the fsaverage template based on cortical folding patterns.

Further preprocessing steps were performed using Python scripts based on PyMVPA (Hanke et al., 2009; [http://www.py\\_mvpa.org/](http://www.py_mvpa.org/)). First, functional data were further downsampled to a standard cortical surface mesh with 18,742 vertices across both hemispheres (3 mm vertex spacing; 20,484 vertices before removing non-cortical vertices), and data acquired during overlapping movie segments were discarded (8 TRs, 20 s, for each of runs 2–8). Then, nuisance regressors—6 motion parameters and their derivatives, global signal, framewise displacement

(Power et al., 2014), 6 principal components from cerebrospinal fluid and white matter (aCompCor; Behzadi et al., 2007), and up to second order polynomial trends—were partialled out from functional data separately for each run. Finally, the residual time series of each surface vertex in each run was normalized to zero mean and unit variance.

2.5. Hyperalignment

First, we created a common representational space to hyperalign

functional data based on an independent dataset. The dataset comprised responses to the same movie from 11 different participants (Guntupalli et al., 2016; Haxby et al., 2011). We preprocessed the 11 participants' data through the same pipeline, and hyperaligned responses to the entire movie for all subjects using searchlight hyperalignment (Guntupalli et al., 2016) with a 20-mm searchlight radius. For a given searchlight, the hyperalignment algorithm uses the Procrustes transformation to rotate each subject's feature space so as to best align response trajectories across individuals. The local transformations for each searchlight are then

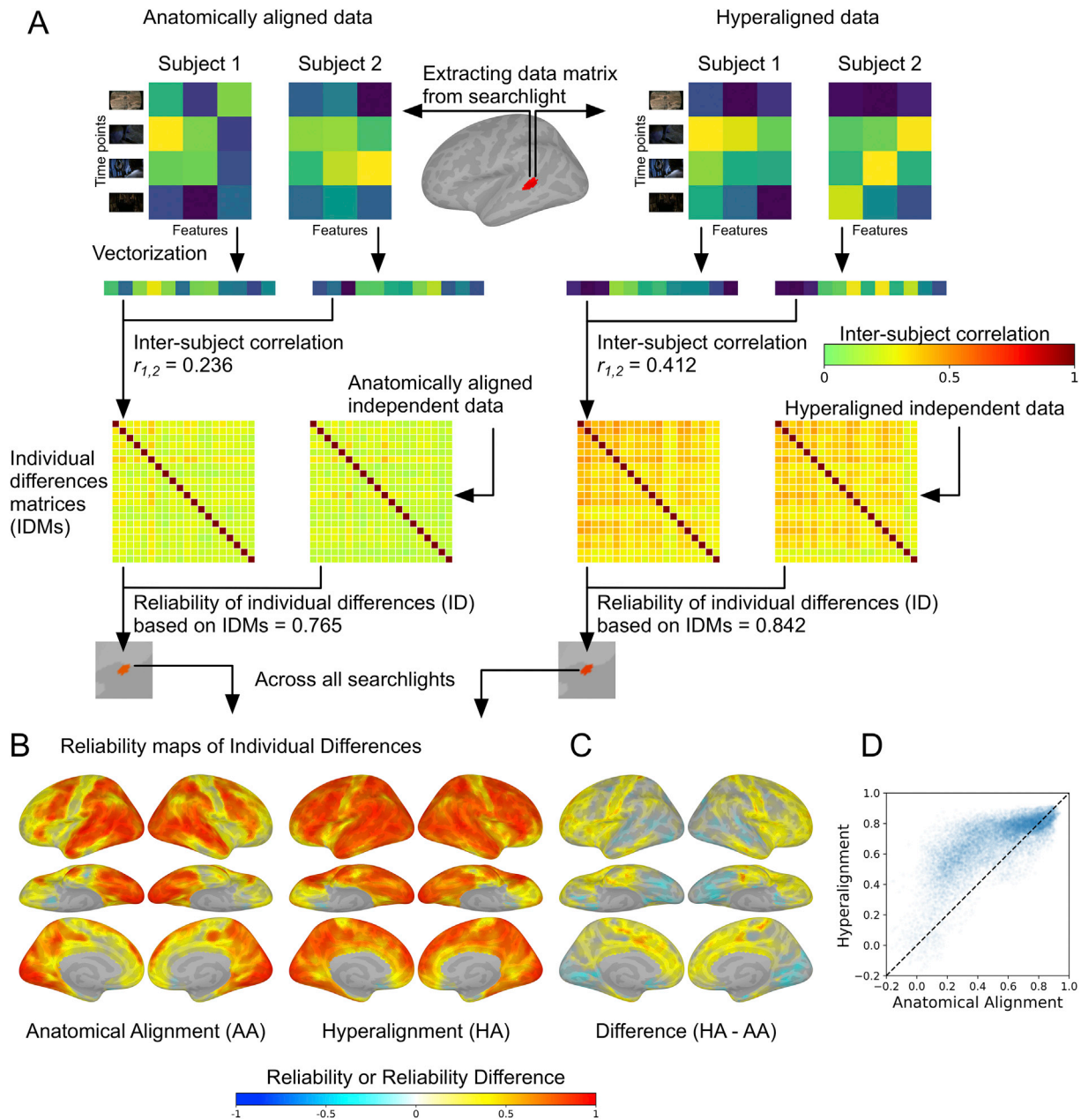


**Fig. 1.** Measuring the reliability of individual differences in local response profiles. (A) Schematic illustration of the analysis pipeline. Using either anatomically-aligned or hyperaligned data, within each searchlight, a time-points (i.e., TRs) by features (i.e., vertices) data matrix was extracted from each subject, and vectorized into a vector of response profiles. The similarity (i.e., correlation) of the vectors for each pair of subjects was computed, forming a subjects-by-subjects similarity matrix (individual differences matrix; IDM) capturing individual differences. Two IDMs were obtained based on independent data (responses to two different parts of the movie) from the same group of people, and the reliability of individual differences was measured as the correlation of their vectorized upper triangles. Note that we used a similar procedure to measure the reliability of individual differences in functional connectivity patterns and representational geometries (see text for details and Fig. 2). (B) Reliability maps of individual differences. These maps depict the searchlight reliabilities of individual differences in local response profiles based on anatomically-aligned data (left) and hyperaligned data (right). (C) Map of reliability difference between hyperaligned data and anatomically-aligned data. (D) Scatterplot of searchlight reliabilities of IDMs in anatomically-aligned data (x-axis) and hyperaligned data (y-axis). In general, individual differences are more reliable with hyperaligned data. Most searchlights (82.1%) showed an increase in the reliability of individual differences with hyperalignment, and the average reliability across all searchlights increased from 0.540 to 0.693.

aggregated, forming a single, sparse transformation matrix for each cortical hemisphere. The hyperaligned data of the 11 participants were then averaged and normalized to unit variance to serve as the final common representational space.

Then, we derived hyperalignment transformations for each of the 20 participants to the common representational space based on their responses to the first half of the movie (runs 1–4), and applied these transformations to data from the second half of the movie (runs 5–8). The following analyses of individual differences were based on the second half of the movie for these 20 participants, and are thus completely independent of the data used for deriving the common space and hyperalignment parameter estimation. Note that all data were anatomically aligned according to sulcal curvature on the cortical surface prior to hyperalignment (see 2.4).

## 2.6. Indexing local functional architecture

We measured individual differences in local functional architecture based on three functional indices that are commonly used in the neuroimaging literature: response profiles, functional connectivity (Biswal et al., 1995), and representational geometry (Kriegeskorte and Kievit, 2013; Kriegeskorte et al., 2008). Based on a surface-based searchlight analysis (Kriegeskorte et al., 2006; Oosterhof et al., 2011), for each individual and each searchlight (9 mm radius), the multivariate neural signature based on a given functional index is represented as a vector, and the difference between a pair of individuals can be quantified as the dissimilarity between their neural signature vectors (Fig. 1A).

We use the term “response profile” to refer to the response time series to a part of the movie for each feature in searchlight. The response profiles of all features in the searchlight formed a time-points by features data matrix for each individual. This data matrix was vectorized into a vector of response profiles reflecting the spatiotemporal pattern of an individual's responses to the movie. We computed the functional connectivity profile of each feature as the Pearson correlation between its response time series and the response time series for all 18,742 features in the brain, which reflects its co-activation pattern with those 18,742 connectivity targets. The functional connectivity profiles of all features in a searchlight formed a connectivity targets by features matrix, which can be vectorized and compared across individuals. We computed the representational geometry of each searchlight as a time-point-based representational dissimilarity matrix (RDM; Guntupalli et al., 2016; Kriegeskorte et al., 2008) based on correlation distance. That is, for each searchlight we first computed a time-points by time-points RDM. For example, the first part of the movie (runs 5–6) contains 668 time points, and that yields a  $668 \times 668$  RDM per individual per searchlight, and each entry in the matrix reflects the correlation distance ( $1 - r$ ) between the spatial patterns for two time points in that searchlight. Then, the similarity between each pair of individuals was measured as the correlation between vectorized upper triangles of the RDMs.

## 2.7. Measuring the reliability of individual differences

Within each searchlight, we modeled individual differences in local cortical functional architecture as a 20 subjects  $\times$  20 subjects similarity matrix, which we refer to as an individual differences matrix (IDM). Each entry in an IDM is the similarity (i.e., Pearson correlation) between neural signature vectors of a given functional index (see 2.6) for a pair of individuals. By modeling the similarity structure (Kriegeskorte and Kievit, 2013) between individuals, IDMs can be compared across different stimuli (e.g., different parts of the movie data) and different functional indices.

We utilized this feature of IDMs and assessed the reliability of individual differences by comparing IDMs based on different parts of the movie data. Within each searchlight, we split responses to the second

half of the movie into two parts (runs 5–6, 7–8), computed an IDM from each part, and evaluated the reliability of the individual differences structure by comparing the two matrices. See Fig. 1A for a schematic of this procedure. Because IDMs are symmetric and the diagonals are not informative, we quantified reliability as the Pearson correlation between the vectorized upper triangles of the IDMs. The reliability values from all searchlights form a reliability map of individual differences.

Using each of the functional indices, we obtained two reliability maps of individual differences, one based on anatomically-aligned data and the other based on hyperaligned data. To simplify the comparison between reliability maps, we first focused on comparing the average reliability difference across all searchlights. Then, we counted the percentage of searchlights that showed the same direction of effect as the average reliability. If the average reliability based on one alignment method is higher, and the reliabilities in most searchlights are also higher with the same alignment method, then the average reliability difference is not likely to be driven by outlier searchlights, and the average reliability difference is a good summary statistic for the reliability maps. We used bootstrap tests to estimate confidence intervals (CIs) and statistical significance. In each of 20,000 repetitions, we randomly sampled a group of 20 individuals by sampling with replacement from the 20 original individuals, then computed IDMs based on the bootstrapped sample, and obtained statistics accordingly, such as average reliability and average reliability difference. During bootstrapping, non-informative correlation values originally in the diagonal of an IDM (self-similarity values of 1 for a given participant due to sampling with replacement) may appear in off-diagonal cells, so we excluded these values (less than 5%) from the upper triangles to avoid overestimation of reliability values (Kriegeskorte et al., 2008). The 95% CI of a statistic is estimated as the 2.5th and 97.5th percentiles of the statistic from the bootstrapped samples (i.e., the sampling distribution of the statistic estimated by bootstrapping subjects), and the  $p$ -value is estimated based on the percentile rank of a null hypothesis score (e.g., average reliability difference of 0) compared with the estimated sampling distribution.

## 2.8. Separating coarse-scale and fine-scale individual differences

We divided the information in those functional indices into coarse-scale information and fine-scale information, to test if the alignment method used affects individual differences differently based on the spatial scale of topographic functional information.

When using response profiles as the functional index, we defined coarse-scale information as the mean response profile (time series) across all features in a searchlight, and fine-scale information as the pattern residuals after subtracting the searchlight mean response profile from each feature's response profile. In this case, the remaining pattern only contains fine-scale information and no variation of mean response across movie time-points. When using functional connectivity as the functional index, we defined coarse-scale information as the correlations between the searchlight mean response profile and those from the 18,742 connectivity targets, and the fine-scale information as the correlations between the residual time series of the features and those of the targets. We measured representational geometry as correlation distances between spatial patterns of different movie time-points. Correlations between spatial patterns implicitly remove the mean and standard deviation across features (Misaki et al., 2010), and thus only use fine-scale information. Therefore, we didn't perform this analysis with representational geometry.

## 2.9. Comparing functional indices

We then compared IDMs based on different functional indices to see if the structure among individuals based on one functional index was retained for the other functional indices. Thus, instead of comparing

**Table 1**

Comparison of reliability of individual differences in local cortical functional architecture between anatomically-aligned (AA) and hyperaligned (HA) data, based on response profiles, functional connectivity, or representational geometry. For all three functional indices, most searchlights had higher reliability of individual differences for hyperaligned data than for anatomically-aligned data (i.e., (HA > AA)% larger than 50%), and the mean reliability across all searchlights was higher for hyperaligned data (i.e., Mean (HA – AA) larger than 0). Numbers in brackets denote 95% confidence intervals obtained by bootstrapping subjects.

Reliability of Individual Differences in Local Cortical Functional Architecture				
Functional Index	Mean (AA)	Mean (HA)	(HA > AA)%	Mean (HA – AA)
Response Profiles	0.540 [0.446, 0.585]	0.693 [0.578, 0.744]	82.10%	0.153 [0.116, 0.182], $p < 0.0001$
Functional Connectivity	0.799 [0.750, 0.827]	0.861 [0.808, 0.894]	72.70%	0.062 [0.020, 0.106], $p = 0.0079$
Representational Geometry	0.472 [0.387, 0.499]	0.601 [0.482, 0.657]	77.50%	0.129 [0.089, 0.166], $p < 0.0001$

IDMs from different parts of the movie data based on the same functional index (as in the reliability analysis, see 2.7; e.g., index 1 movie part 1 vs. index 1 movie part 2), we compared IDMs from different parts of the movie based on different functional indices. In this approach, two correlation coefficients can be obtained from each pair of functional indices (index 1 movie part 1 vs. index 2 movie part 2, and index 1 movie part 2 vs. index 2 movie part 1). We averaged these two correlation coefficients to reduce estimation error.

### 3. Results

#### 3.1. Reliability of individual differences

We computed searchlight maps of the reliability of individual differences in response profiles, functional connectivity, and representational geometry using both anatomically-aligned data and hyperaligned data. Each location on the cortical surface is assigned a correlation value (ranging from -1 to 1) denoting the reliability of individual differences for a given functional index in that searchlight. Note that we expect most reliabilities to be positive, and that negative and near-zero reliabilities are indicative of noise.

The average reliability of individual differences based on response profiles across all searchlights increased significantly from 0.540 for anatomically-aligned data to 0.693 for hyperaligned data (Fig. 1; see Table 1 for statistics). Most searchlights (82.1%) had higher reliability with hyperalignment, consistent with the searchlight average results, indicating that the increase in average reliability was not due to outlier searchlights. Increases in reliability for hyperaligned data were largest in prefrontal cortices, both lateral and medial, where reliabilities were low for anatomically-aligned data (Fig. 1C). By contrast, increases in reliability were smallest in occipital and temporal visual cortices, temporal auditory cortex, and the frontal eye field, where reliabilities were high for anatomically-aligned data. Reliabilities in somatosensory and motor areas in pre- and postcentral gyri also were boosted by hyperalignment but were low for both anatomically and hyperaligned data.

The average reliability of individual differences based on functional connectivity (Fig. 2, upper; Table 1) across all searchlights increased significantly from 0.799 for anatomically-aligned data to 0.861 for hyperaligned data. Across all searchlights, 72.7% had higher reliability

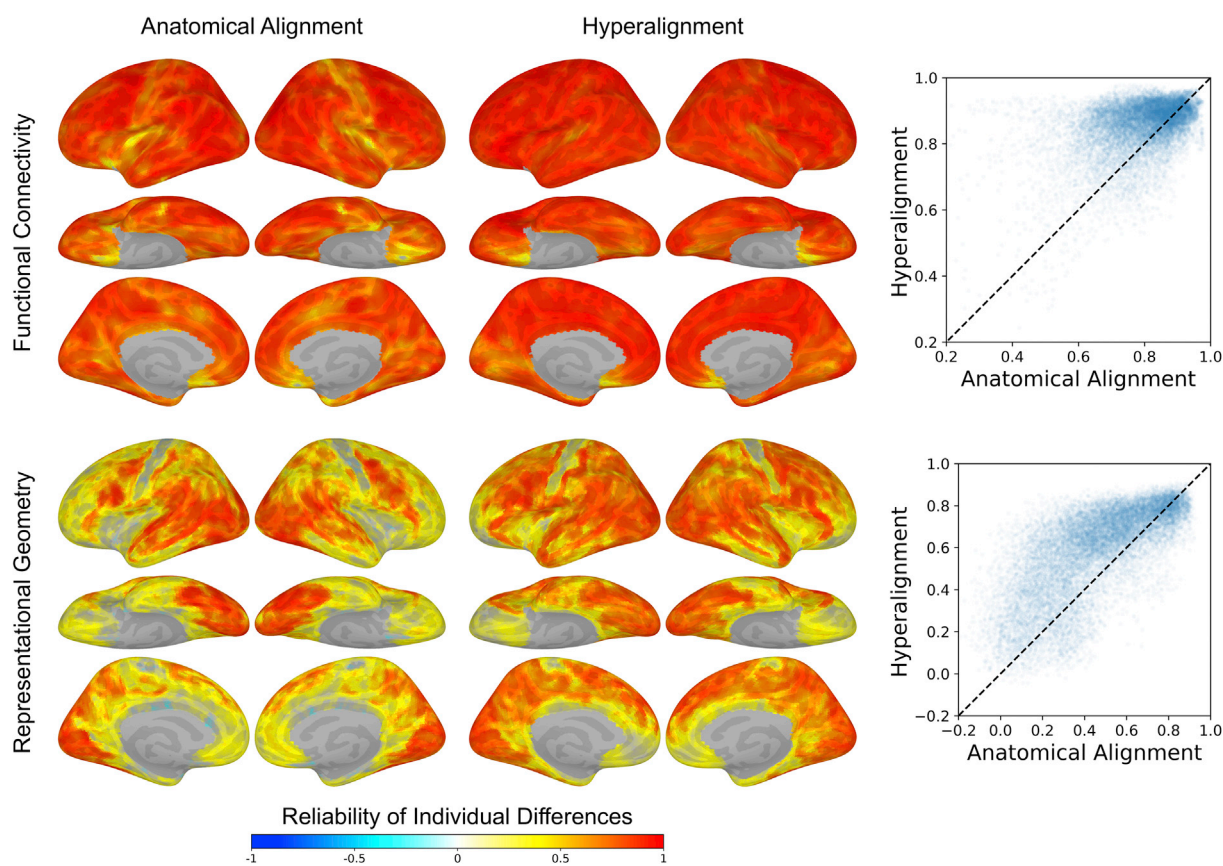


**Fig. 2.** The reliability of individual differences indexed by functional connectivity (upper) and representational geometry (lower). When using functional connectivity to index individual difference, 72.7% searchlights had higher reliability with hyperalignment, and the average reliability increased from 0.799 to 0.861. When using representational geometry, 77.5% had higher reliability with hyperalignment, and the average reliability increased from 0.472 to 0.601.

with hyperalignment.

The average reliability of individual differences based on representational geometry (Fig. 2, lower; Table 1) across all searchlights increased from 0.472 with anatomically-aligned data to 0.601 with hyperaligned data. Across all searchlights, 77.5% had higher reliability with hyperalignment.

IDMs based on anatomically-aligned data and hyperaligned data were moderately correlated for all three functional indices. The average correlation was 0.419 when using response profiles as the functional index, 0.371 when using functional connectivity as the index, and 0.365 when using representational geometry as the functional index. Note that the highest possible correlation between IDMs is constrained by the reliability of IDMs based on each alignment method. As a result searchlights having a higher noise ceiling are more likely to have a higher correlation between anatomically-aligned IDM and hyperaligned IDM. The spatial correlation between the correlation map and the noise ceiling map was 0.748 for response profiles, and 0.841 for representational geometry, but only 0.065 for functional connectivity, probably due to the uniformly high reliabilities for this index. IDMs based on anatomically-aligned data also reflect individual differences in topography that are factored out in hyperaligned data, which may further reduce correlations between IDMs for these two alignment methods. The influence of topography-based individual differences may be especially strong for functional connectivity which reflects both the topography of vertices within searchlights and the topography of vertices that are the connectivity targets out of each searchlight.

In summary, the reliability of individual differences in response profiles, functional connectivity, and representational geometry all became more reliable after hyperalignment. Across the three functional indices, individual differences in functional connectivity were more reliable than individual differences in response profiles, and individual differences in response profiles were more reliable than individual differences in representational geometry. Based on anatomically-aligned data, 91.2% of searchlights had higher reliability for functional connectivity compared with response profiles, and the average difference across all searchlights was 0.260 (95% CI was [0.205, 0.344] based on bootstrapping subjects); 65.5% of searchlights had higher reliability for response profiles compared with representational geometry, and the average difference across searchlights was 0.068 [0.043, 0.103]. Based on hyperaligned data, 92.8% of searchlights had higher reliability for functional connectivity compared with response profiles, and the average difference across all searchlights was 0.168 [0.110, 0.267]; 75.6% searchlights had higher reliability for response profiles compared with representational geometry, and the average difference across searchlights was 0.092 [0.067, 0.126].

### 3.2. Coarse-scale and fine-scale individual differences

We separated the information encoded in each searchlight into coarse and fine spatial scales, and assessed the reliability of individual differences for both. Coarse-scale information is defined as the average time series across all cortical features within a searchlight (regional-average response profile) and the correlations of the searchlight average time series with functional connectivity targets (regional-average connectivity profile), and the fine-scale information is based on the residuals of the data matrix after removing the searchlight average time series or average functional connectivity vector. These approaches characterized independent and complementary types of information encoded in each searchlight.

When using response profiles to index individual differences (Fig. 3, upper; Table 2), the average reliability based on coarse-scale information marginally increased from 0.496 with anatomically-aligned data to 0.528 with hyperaligned data. Across all searchlights, 58.8% had higher reliability with hyperalignment. By contrast, the average reliability based on fine-scale information increased significantly from 0.415 with anatomically-aligned data to 0.660 with hyperaligned data. Across all

searchlights, 92.5% had higher reliability with hyperalignment.

When using functional connectivity to index individual differences (Fig. 3, lower; Table 2), the average reliability based on coarse-scale information was similar for anatomically-aligned data (0.726) and hyperaligned data (0.730). Across all searchlights, 48.2% had higher reliability with hyperalignment. The average reliability based on fine-scale information increased significantly from 0.782 with anatomically-aligned data to 0.865 with hyperaligned data. Among all searchlights, 81.3% had higher reliability with hyperalignment.

The reliability of fine-scale individual differences benefited more from hyperalignment than did the reliability of coarse-scale individual differences (Fig. 4 and Table 2). When using response profiles to index individual differences, the increases in average reliability with hyperalignment were significantly larger for fine-scale data (mean increase = 0.246) than for coarse-scale data (mean increase = 0.032). Hyperalignment yielded a larger increase in the reliability of fine-scale individual differences in 88.9% of searchlights. When using functional connectivity to index individual differences, the increases in average reliability again were significantly larger for fine-scale data (0.083 versus 0.004, respectively). Across all searchlights, 71.4% had a larger increase in the reliability of fine-scale individual differences in functional connectivity. Note with both functional indices, fine-scale individual differences based on hyperaligned data had the highest average reliability among the four combinations, thus the smaller increase in the reliability of coarse-scale individual differences was not due to ceiling effects.

### 3.3. Agreement across functional indices

We next correlated IDMs based on different functional indices derived from different parts of the movie data (Fig. 5; Table 3). A positive correlation indicates that individuals who differ more according to one functional index are also likely to differ more according to the other functional index, and individuals who are more similar on one index are also more similar on the other index. Inter-index correlations computed across the two parts of the movie were then averaged. Consequently, the similarity of IDMs based on different indices is derived from different parts of the movie for each index.

When comparing individual differences in response profiles and individual differences in functional connectivity, the average correlation across all searchlights increased significantly from 0.408 for anatomically-aligned data to 0.582 for hyperaligned data. Among all searchlights, 83.8% had higher correlations with hyperaligned data.

When comparing individual differences in response profiles and individual differences in representational geometry, the average correlation across all searchlights increased significantly from 0.272 for anatomically-aligned data to 0.554 for hyperaligned data. Among all searchlights, 96.5% had higher correlations with hyperaligned data.

When comparing individual differences in functional connectivity and individual differences in representational geometry, the average correlation across all searchlights increased significantly from 0.077 for anatomically-aligned data to 0.415 for hyperaligned data. Among all searchlights, 96.8% had higher correlations with hyperaligned data.

Compared with anatomically-aligned data, more searchlights had positive inter-index IDM correlations with hyperaligned data, and the average correlation across all searchlights increased. Thus, after hyperalignment, all three functional indices converged on more congruent characterizations of inter-subject similarity of cortical functional architecture.

## 4. Discussion

In this study, we measured individual differences in local cortical functional architecture based on three functional indices—response profiles, functional connectivity, and representational geometry—using dynamic, naturalistic movie stimuli. We quantified individual differences with IDMs. Each IDM provides an index of the similarity structure among

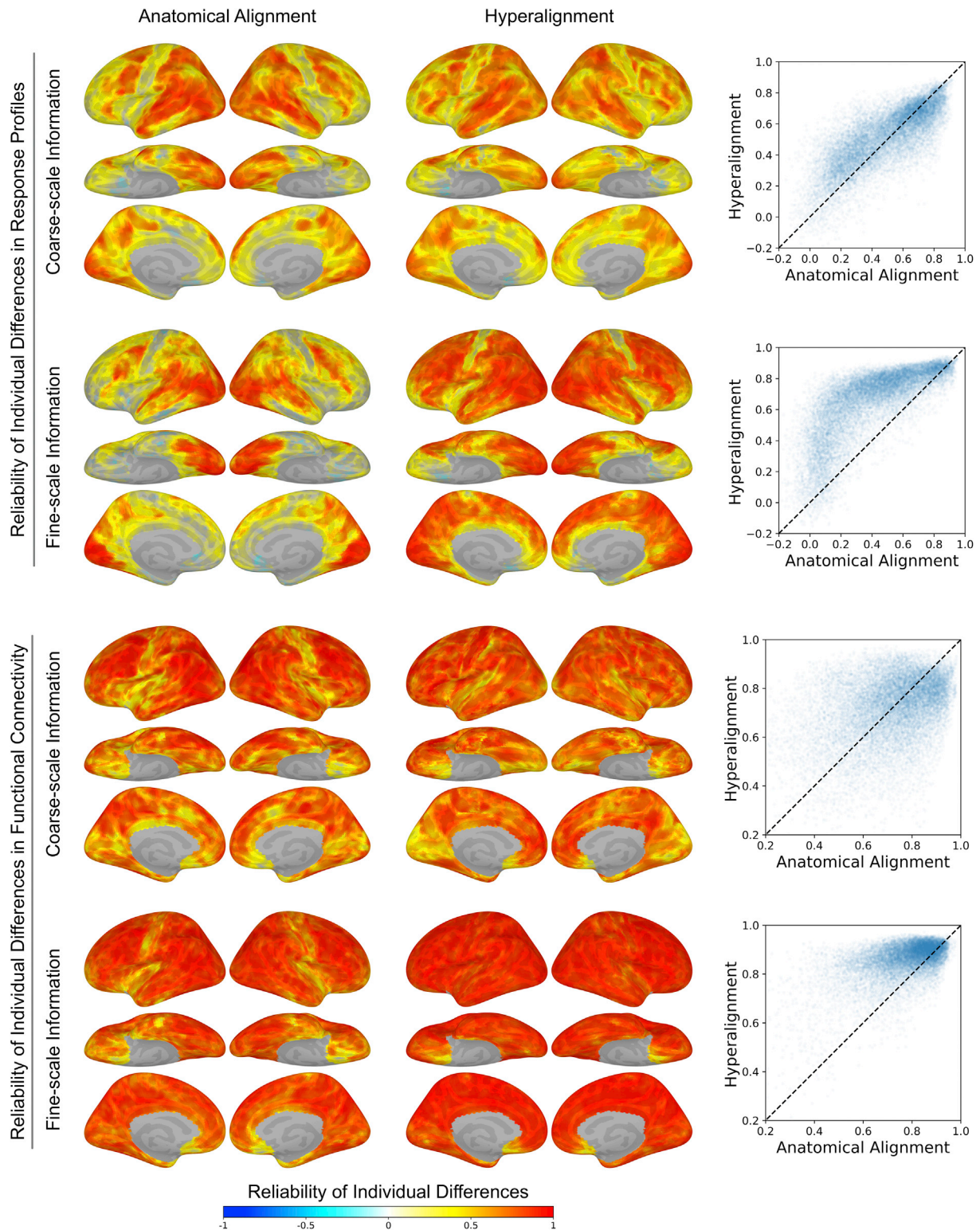


**Fig. 3.** Individual differences at coarse and fine spatial scales. We separated coarse-scale information (regional-average response profiles or regional-average connectivity profiles) and fine-scale information (pattern residuals after removing coarse-scale information) from the functional indices, and modeled individual differences accordingly. When using response profiles to index individual differences, hyperalignment increased the average reliability of coarse-scale individual differences from 0.496 to 0.528, and that of fine-scale individual differences from 0.415 to 0.660. When using functional connectivity, hyperalignment increased the average reliability of coarse-scale individual differences from 0.726 to 0.730, and that of fine-scale individual differences from 0.782 to 0.865. In general, the reliability of fine-scale individual differences benefited more from hyperalignment than did coarse-scale individual differences.

**Table 2**

Reliability of individual differences in local cortical functional architecture at different spatial scales. Coarse-scale information reflects the average response or connectivity profile across all vertices in a searchlight (i.e., spatial averaging), and fine-scale information reflects spatial response or connectivity patterns that are not captured by the average response/connectivity profile. The increase in reliability was marginal for coarse-scale information, but much larger for fine-scale information.

Reliability of Individual Differences in Local Cortical Functional Architecture at Different Spatial Scales					
Functional Index	Spatial Scale	Mean (AA)	Mean (HA)	(HA > AA)%	Mean (HA – AA)
Response Profiles	Coarse	0.496 [0.400, 0.542]	0.528 [0.411, 0.590]	58.80%	0.032 [0.000, 0.059], $p = 0.0493$
	Fine	0.415 [0.348, 0.455]	0.660 [0.538, 0.714]	92.50%	0.246 [0.181, 0.282], $p < 0.0001$
Functional Connectivity	Coarse	0.726 [0.679, 0.749]	0.730 [0.673, 0.772]	48.20%	0.004 [-0.044, 0.057], $p = 0.7960$
	Fine	0.782 [0.754, 0.792]	0.865 [0.810, 0.898]	81.30%	0.083 [0.040, 0.121], $p = 0.0027$

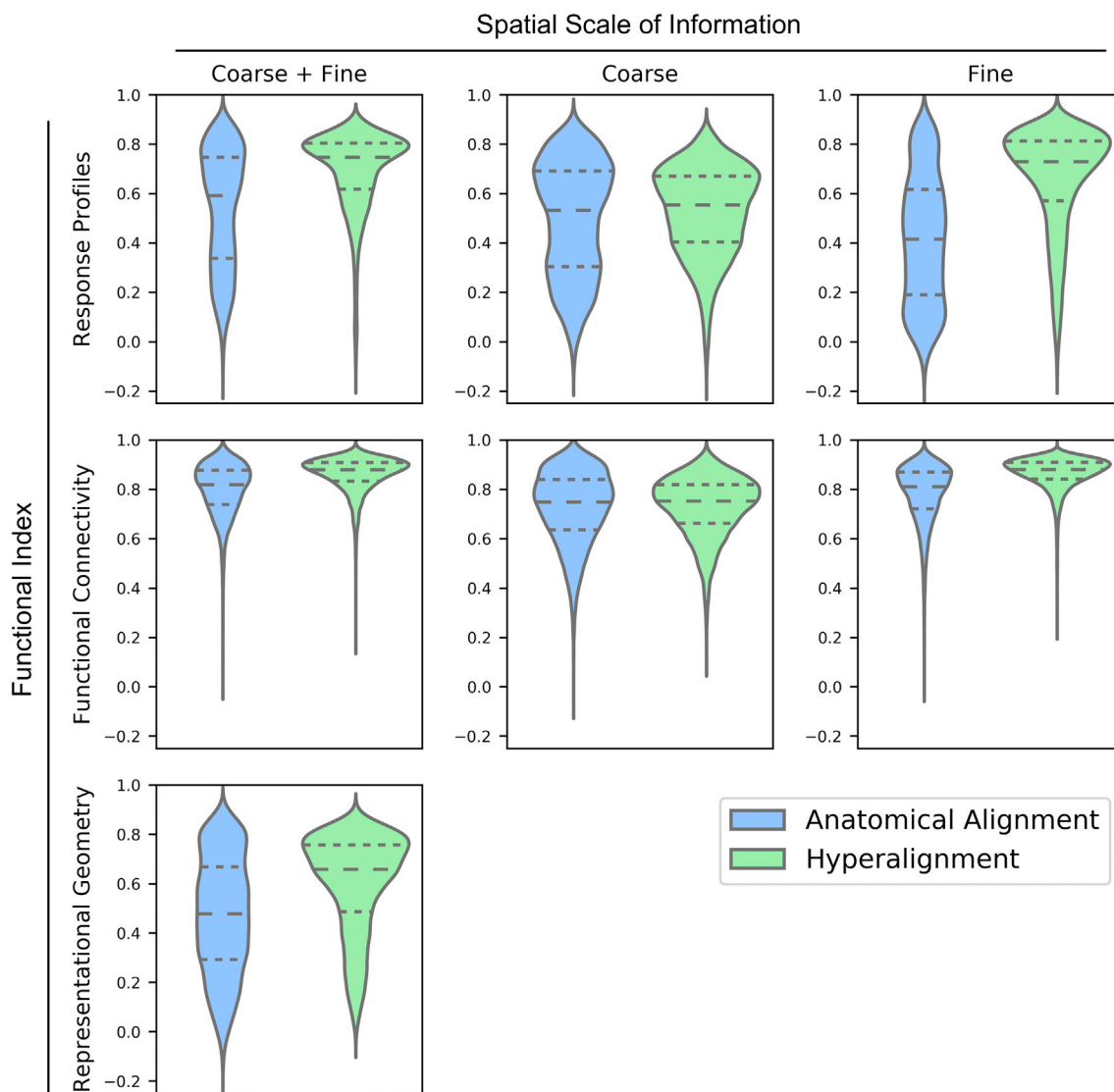


**Fig. 4.** Distribution of searchlight reliabilities of individual differences across functional indices, spatial scales, and alignment methods. With hyperalignment, individual differences were more reliable across all three functional indices (left column, see also Figs. 1B and 2). When only coarse-scale information was used, the distribution of reliabilities was similar for both alignment methods (middle column, see also Fig. 3). By contrast, when only fine-scale information was used, the distribution of reliabilities shifted toward higher values with hyperalignment (right column, see also Fig. 3). Dashed lines denote quartiles of each distribution.

individuals, which can be thought of as an individual-differences geometry. IDMs derived from different parts of the movie or from different functional indices can be compared directly. These IDMs capture neural similarities among subjects. The relationship of these individual differences in cortical functional architecture to phenotypic variation is beyond the scope of this study—however, reliable neural IDMs can be considered a precondition for relating individual differences in neural function to these other variables (Castellanos et al., 2013; Dubois and

Adolphs, 2016; Gabrieli et al., 2015; Van Horn et al., 2008; Woo et al., 2017). We assessed the reliability of individual differences by comparing IDMs from different parts of the movie, and found reliable individual differences in all three functional indices throughout cortex. Naturalistic stimuli are engaging and content-rich, evoking a variety of brain states and facilitating the detection of individual differences (Vanderwal et al., 2017). Importantly, after aligning each individual's data to a common space using hyperalignment, we found individual differences in all three

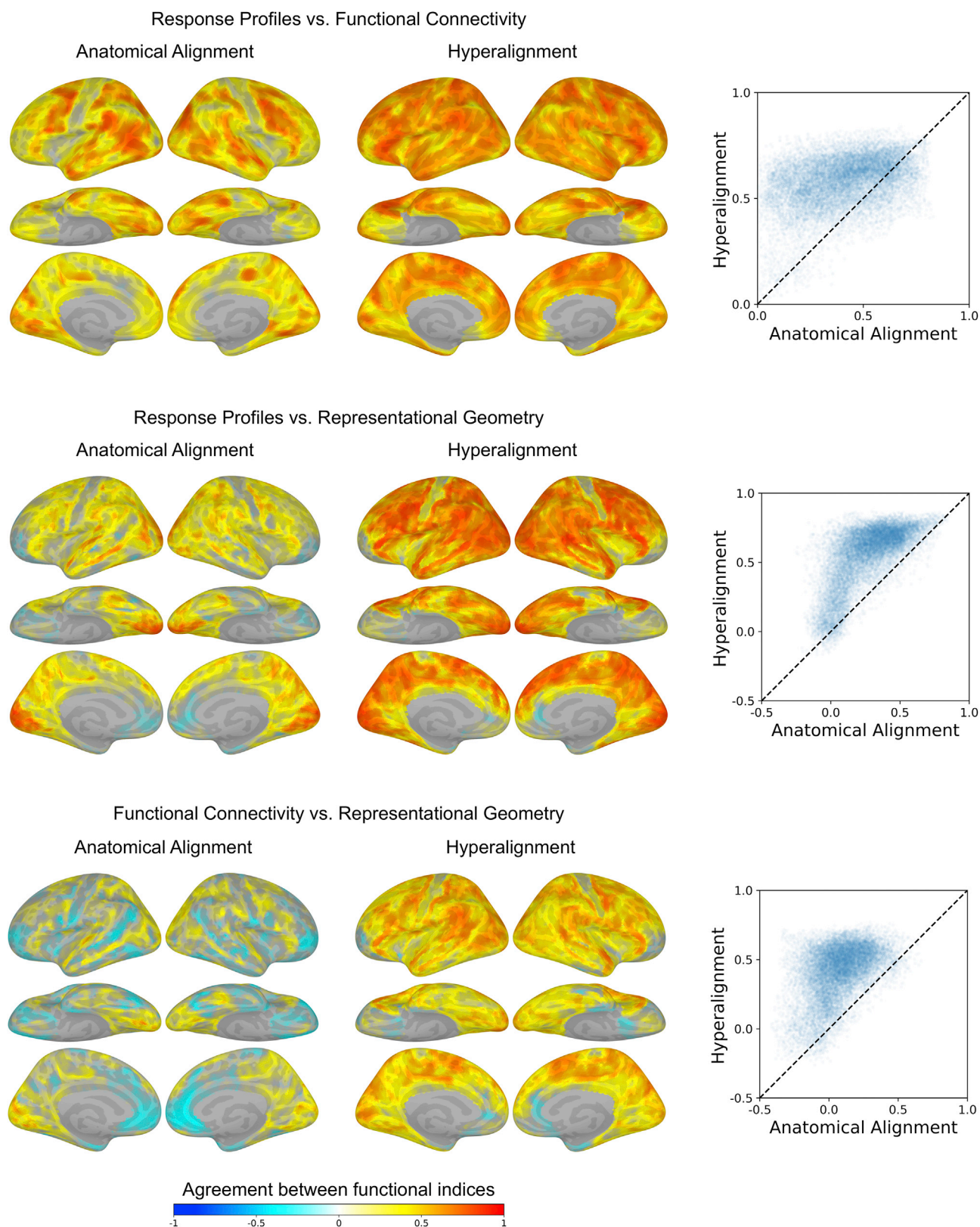


**Fig. 5.** Agreement of individual differences across functional indices. Within each searchlight, we computed the correlation between two IDMs based on different functional indices and different parts of the movie data, and averaged that across permutations of movie parts. A positive correlation means that individuals who differ more according to one functional index are likely to differ more for the other functional index. The average correlation between response profile IDMs and functional connectivity IDMs was 0.408 for anatomically-aligned data, and 0.582 for hyperaligned data. The average correlation between response profile IDMs and representational geometry IDMs was 0.272 for anatomically-aligned data, and 0.554 for hyperaligned data. The average correlation between functional connectivity IDMs and representational geometry IDMs was 0.077 for anatomically-aligned data, and 0.415 for hyperaligned data.

**Table 3**

Agreement of individual differences across functional indices. The average correlation of IDMs from different functional indices was positive for all pairs of functional indices, and the average correlation was higher for hyperaligned data. This indicates that individuals who differed along one functional index tend to differ for others, and are more likely to differ after hyperalignment.

Agreement of Individual Differences across Functional Indices					
Functional Indices		Mean (AA)	Mean (HA)	(HA > AA)%	Mean (HA-AA)
Response Profiles	Functional Connectivity	0.408 [0.334, 0.465]	0.582 [0.454, 0.668]	83.80%	0.174 [0.093, 0.247], $p < 0.0001$
Response Profiles	Representational Geometry	0.272 [0.203, 0.317]	0.554 [0.422, 0.626]	96.50%	0.281 [0.216, 0.315], $p < 0.0001$
Functional Connectivity	Representational Geometry	0.077 [0.018, 0.135]	0.415 [0.263, 0.520]	96.80%	0.338 [0.229, 0.417], $p < 0.0001$

functional indices become even more reliable; hyperalignment increased reliability in a clear majority of searchlights (73%–82%) and increased average reliability across all searchlights. This suggests individuals differ reliably in local cortical functional architecture, but that these differences can be obscured by suboptimal alignment of brain imaging data across individuals.

To further test this hypothesis, we divided the information in these functional indices into coarse-scale information and fine-scale information, and assessed the reliability of individual differences accordingly. Coarse-scale information was computed based on the average time series of all vertices in a searchlight, and thus was spatially smooth and relatively robust against misalignment of data across individuals (conceptually related to the motivation for spatially smoothing functional data in multi-subject univariate analyses; Petersson et al., 1999; Carp, 2012). The information not captured by searchlight average time series, i.e., the residual time series in each cortical vertex, was defined as fine-scale information, and thus was independent and orthogonal to coarse-scale information. Coarse-scale information is typically used to link a large brain region with the presence of a stimulus category (or contrasts between categories). For example, the average response magnitude of a large patch of fusiform gyrus is sufficient for determining whether a face or a house stimulus is being presented (Kanwisher et al., 1997), but not sufficient for discriminating between face identities, head angles, or the faces of different species of primates. In contrast, fine-scale information of this kind (e.g., between species of birds or between nearby time segments of a continuous movie stimulus) is encoded in complex, finer-grained response topographies (Connolly et al., 2012; Guntupalli et al., 2017; Haxby et al., 2011; Nastase et al., 2017; Sha et al., 2015). We found the reliability of coarse-scale individual differences was the same or slightly increased with hyperalignment. In contrast, the reliability of fine-scale individual differences increased dramatically with hyperalignment, and surpassed the reliability of coarse-scale individual differences. These results suggest individual differences in local cortical functional architecture exist at both coarse and fine spatial scales. However, individual differences in fine-scale functional architecture can only be efficiently captured when data are properly aligned across individuals. This is a critical development for identifying biomarkers, as some abnormalities may not be evident in coarse-grained functional organization and only manifest at fine spatial scales (Woo et al., 2017; cf. Hackmack et al., 2012).

It is essential to establish functional correspondence across individuals before analyzing how they differ in cortical functional architecture. Consider measuring a single brain feature (e.g., voxel, vertex, electrode, etc.) at the same macroanatomical position in two individuals that responds preferentially to different kinds of stimuli. The two individuals' response time series would be highly similar if the two kinds of stimuli always co-occur, and highly dissimilar if the two kinds of stimuli always appear in an interleaved fashion. In these scenarios, measured individual differences in cortical functional architecture are prone to the co-occurrence and frequency of stimuli, and less generalizable to new tasks and new sets of stimuli. On the other hand, if the same brain feature from the two individuals are from a common functional space (e.g., common space created by hyperalignment), they are expected to share similar functional properties like response tuning profiles or functional connectivity profiles. In this case, measured individual differences in

cortical functional architecture will be robust against variations in stimuli, and thus more generalizable and reliable.

Consider the same brain feature with differential response tuning across two individuals. Is this discrepancy due to topographic differences? The mismatch may be due to differences in functional–anatomical correspondence across individuals, or the way in which a particular subject's brain signals were sampled (e.g., the discretization of brain signals into voxels). In this simplistic example, the discrepancy may be resolved simply by remapping one feature to another nearby feature across individuals. Hyperalignment, and related approaches (e.g., Yamada et al., 2015), relax this one-to-one mapping and flexibly account for topographic differences by modeling the responses of a given feature as a weighted sum of nearby features in the common space. If, after hyperalignment, the discrepancy remains, this is strongly indicative of a feature in a particular individual that deviates from the group model for the cortical field to which that feature belongs. In a multivariate context, this would be reflected in individual differences in representational geometry (Charest et al., 2014). By accounting for idiosyncrasies in functional–anatomical correspondence, hyperalignment offers a rigorous framework for modeling deviations from the group and a less-confounded view of individual differences in function.

At first glance, one might expect that hyperalignment, by minimizing individual differences in functional–anatomical correspondence, would produce less reliable individual differences. Hyperalignment does in fact increase similarities among individuals for the functional indices we use (Guntupalli et al., 2016, 2018; Haxby et al., 2011), but nonetheless enhances the structure of the similarities among individuals. The hyperalignment implementation used in this paper uses Procrustes transformations within searchlights, which is a rotation in searchlight high-dimensional feature spaces. It re-distributes variances across features rather than changing the variances themselves. Therefore, the Procrustes transformation is expected to correct for individual differences in topographic distributions of function while maintaining individual differences in function per se. For example, if one individual's response magnitude to a stimulus is twice as high as another individual, or if the response exists in twice as many features, such differences will still be retained in Procrustes-transformed data. However, if two individuals have the same response but the response exists in different features, their differences will be resolved by the transformation. Therefore, by projecting each individual's data into the common space, we can measure differences in functional tuning without confounds from (mis)localization of function.

Searchlight hyperalignment (Guntupalli et al., 2016) adds local Procrustes transformations together to form a whole-brain transformation matrix. When a feature is included in multiple searchlights, respective transformations are combined. This procedure is related to ensemble learning techniques (Zhou, 2012) in that it boosts the shared part of the transformations and suppresses the noisy part. Therefore, instead of a completely orthonormal whole-brain transformation matrix, it provides a more accurate and robust whole-brain transformation. As a result, the signal shared across individuals will be boosted and the noise suppressed; this may partly explain why individual differences in cortical functional architecture become even more reliable after searchlight hyperalignment.

Representational geometry (Kriegeskorte and Kievit, 2013) measures

the structure of similarities between stimulus representations, which itself is not expected to change with rotations in the feature space (e.g., the Procrustes transformation). However, variances in a searchlight after hyperalignment are not identical to the variances in the searchlight in anatomically-aligned data. Small differences in representational geometry may be observed after searchlight hyperalignment partly because the method for aggregating searchlights will adjust which (and to what extent) features are considered “members” of a given cortical field. This is conceptually analogous to localizing functional regions of interest (ROIs) in univariate analyses (Saxe et al., 2006), and comparing these functional ROIs rather than comparing anatomical ROIs (which increases statistical power and functional resolution; Nieto-Castañón and Fedorenko, 2012). Similarly to functional ROIs, following hyperalignment, representational geometry is computed across individuals in a “functional searchlight” instead of a purely anatomy-based searchlight. However, note the “boundary” of the “functional searchlight” is not an anatomically-defined boundary on surface, but is rather a boundary in a high-dimensional information space determined by a transformation which maps multivariate information from each individual’s anatomical space to the information searchlights in common space. Therefore, measuring individual differences in representational geometry with searchlight hyperalignment also benefits from better alignment of functional architecture and reduced topographic confounds.

Note that the effect of hyperalignment on the reliability of individual differences in functional architecture varies across cortical regions. The increases in reliability after hyperalignment were greatest in lateral and medial prefrontal cortices, where reliabilities were relatively low for anatomically-aligned data. In occipital and temporal visual areas, temporal auditory areas, and the frontal eye fields, reliability even decreased slightly after hyperalignment, but was very high for both anatomically-aligned and hyperaligned data. This is likely because the information encoded in fine-scale topographies is highly similar across subjects and individual differences are dominated by topographic differences rather than the information content. Consequently, when these topographic differences are minimized with hyperalignment, noise around residual individual differences in information content is amplified. For example, these regions usually show the highest inter-subject similarity in representational geometry after both anatomical alignment and hyperalignment (Guntupalli et al., 2016, 2018). Some other regions, such as the motor cortex and the insular cortex, encode information (motor behaviors and interoceptive information, respectively) that are unrelated to our movie watching paradigm. Consistent with previous work using movie stimuli (Guntupalli et al., 2016, 2018; Hasson et al., 2004), task-related activity and individual differences in these regions were weak and inconsistent after both anatomical alignment and hyperalignment.

As hyperalignment factors out topographic differences from functional differences, individual differences in the information encoded in fine-grained topographies, such as neural representations (Charest et al., 2014), can be analyzed. For example, in an fMRI study of story comprehension, Chen et al. (2015) studied differences between two groups that were biased to interpret the same short story differently by providing prior information favoring one of two interpretations. The auditory story was identical for the two groups, so that any group difference in brain responses was due only to interpretation of the text, and this difference was stronger for data that were hyperaligned. This supports the current findings in suggesting that hyperalignment enhances the detection of individual differences in high-level cognition and mental representation which are encoded in fine-scale functional topographies.

Although individual differences in local cortical functional architecture can be based on various functional indices, we found that the structure of individual differences was similar across the three functional indices, especially following hyperalignment. The increased congruency of individual differences across these three indices after hyperalignment is due in part to the simple statistical effect of increased reliability—more reliable measures allow higher correlations among measures. The increased reliability, however, may also reflect stronger weighting of

individual differences in the representation of information after hyperalignment and diminished weighting of individual differences in functional topographies, suggesting that the contribution of variations in functional topography to these indices may diminish congruency across indices for anatomically-aligned data. Note that individual differences in functional topography affect these functional indices to different degrees: representational geometry is designed to be independent of within-area topographic differences (rotations in the feature space); response profiles can be affected by topographic differences to some degree; functional connectivity is most prone to topographic differences, as both features in an area and connectivity targets can be affected by topographic differences. Such effects are expected to be reduced by hyperalignment, and the individual differences measured in the hyperaligned common space mainly reflect functional differences without confounding topographic differences. Each functional index is differentially susceptible to topographic differences and hyperalignment improves agreement across indices by attenuating these topographic differences and capturing differences in the fine-scale information that is encoded in fine-scale topographies.

Hyperalignment yields more reliable measures of individual differences in cortical functional architecture both by reducing confounds from topographic idiosyncrasies and by capturing variation around shared bases for how information is encoded in fine-scale topographic patterns. This is a promising step forward for efforts to link individual differences in brain function to individual differences in behavior. As translational neuroscience matures (Dubois and Adolphs, 2016; Gabrieli et al., 2015; Poldrack, 2017; Woo et al., 2017), hyperalignment will be instrumental in building more detailed, clinically-relevant biomarkers.

## Funding

This work was supported by grants from the National Institute of Mental Health (5R01MH075706) and the National Science Foundation (NSF1607845). Funding to pay the Open Access publication charges for this article was provided by Dartmouth College. The authors declare no competing interests.

## Acknowledgements

We thank Yaroslav O. Halchenko, M. Ida Gobbini, Andrew C. Connolly, Matteo Visconti di Oleggio Castello, and Vassiki Chauhan for helpful discussions.

## References

- Adelstein, J.S., Shehzad, Z., Mennes, M., DeYoung, C.G., Zuo, X.-N., Kelly, C., Margulies, D.S., Bloomfield, A., Gray, J.R., Castellanos, F.X., Milham, M.P., 2011. Personality is reflected in the brain’s intrinsic functional architecture. *PLoS One* 6, e27633. <https://doi.org/10.1371/journal.pone.0027633>.
- Arbabshirani, M.R., Plis, S., Sui, J., Calhoun, V.D., 2017. Single subject prediction of brain disorders in neuroimaging: promises and pitfalls. *Neuroimage* 145, 137–165. <https://doi.org/10.1016/j.neuroimage.2016.02.079>.
- Beatty, R.E., Kenett, Y.N., Christensen, A.P., Rosenberg, M.D., Benedek, M., Chen, Q., Fink, A., Qiu, J., Kwapil, T.R., Kane, M.J., Silvia, P.J., 2018. Robust prediction of individual creative ability from brain functional connectivity. *Proc. Natl. Acad. Sci. U.S.A.* 115, 1087–1092. <https://doi.org/10.1073/pnas.1713532115>.
- Behzadi, Y., Restom, K., Liu, J., Liu, T.T., 2007. A component based noise correction method (CompCor) for BOLD and perfusion based fMRI. *Neuroimage* 37, 90–101. <https://doi.org/10.1016/j.neuroimage.2007.04.042>.
- Biswal, B., Yetkin, F.Z., Haughton, V.M., Hyde, J.S., 1995. Functional connectivity in the motor cortex of resting human brain using echo-planar mri. *Magn. Reson. Med.* 34, 537–541. <https://doi.org/10.1002/mrm.1910340409>.
- Carp, J., 2012. The secret lives of experiments: methods reporting in the fMRI literature. *Neuroimage* 63, 289–300. <https://doi.org/10.1016/j.neuroimage.2012.07.004>.
- Castellanos, F.X., Martino, A.D., Craddock, R.C., Mehta, A.D., Milham, M.P., 2013. Clinical applications of the functional connectome. *Neuroimage* 80, 527–540. <https://doi.org/10.1016/j.neuroimage.2013.04.083>.
- Charest, I., Kievit, R.A., Schmitz, T.W., Deca, D., Kriegeskorte, N., 2014. Unique semantic space in the brain of each beholder predicts perceived similarity. *Proc. Natl. Acad. Sci. U.S.A.* 111, 14565–14570. <https://doi.org/10.1073/pnas.1402594111>.
- Chen, P.-H., Chen, J., Yeshurun, Y., Hasson, U., Haxby, J., Ramadge, P.J., 2015. A reduced-dimension fMRI shared response model. In: Cortes, C., Lawrence, N.D.,

- Lee, D.D., Sugiyama, M., Garnett, R. (Eds.), *Adv. Neural Inf. Process. Syst.*, vol 28. Curran Associates, Inc., pp. 460–468
- Connolly, A.C., Guntupalli, J.S., Gors, J., Hanke, M., Halchenko, Y.O., Wu, Y.-C., Abdi, H., Haxby, J.V., 2012. The representation of biological classes in the human brain. *J. Neurosci.* 32, 2608–2618. <https://doi.org/10.1523/jneurosci.5547-11.2012>.
- Cox, D.D., Savoy, R.L., 2003. Functional magnetic resonance imaging (fMRI) “brain reading”: detecting and classifying distributed patterns of fMRI activity in human visual cortex. *Neuroimage* 19, 261–270. [https://doi.org/10.1016/s1053-8119\(03\)00049-1](https://doi.org/10.1016/s1053-8119(03)00049-1).
- DeYoung, C.G., Hirsh, J.B., Shane, M.S., Papademetris, X., Rajeevan, N., Gray, J.R., 2010. Testing predictions from personality neuroscience. *Psychol. Sci.* 21, 820–828. <https://doi.org/10.1177/0956797610370159>.
- Dubois, J., Adolphs, R., 2016. Building a science of individual differences from fMRI. *Trends Cognit. Sci.* 20, 425–443. <https://doi.org/10.1016/j.tics.2016.03.014>.
- Duncan, K.J., Pattamadilok, C., Knierim, I., Devlin, J.T., 2009. Consistency and variability in functional localisers. *Neuroimage* 46, 1018–1026. <https://doi.org/10.1016/j.neuroimage.2009.03.014>.
- Esteban, O., Markiewicz, C., Blair, R.W., Moodie, C., Isik, A.I., Erramuzpe Aliaga, A., Kent, J., Goncalves, M., DuPre, E., Snyder, M., Oya, H., Ghosh, S., Wright, J., Durme, J., Poldrack, R., Gorgolewski, K.J., 2018. FMRIPrep: a robust preprocessing pipeline for functional mri. *bioRxiv*, 306951. <https://doi.org/10.1101/306951>.
- Fischl, B., 2012. FreeSurfer. *Neuroimage* 62, 774–781. <https://doi.org/10.1016/j.neuroimage.2012.01.021>.
- Fischl, B., Sereno, M.I., Tootell, R.B., Dale, A.M., 1999. High-resolution intersubject averaging and a coordinate system for the cortical surface. *Hum. Brain Mapp.* 8, 272–284. [https://doi.org/10.1002/\(SICI\)1097-0193\(1999\)8:4<272::AID-HBM10>3.0.CO;2-4](https://doi.org/10.1002/(SICI)1097-0193(1999)8:4<272::AID-HBM10>3.0.CO;2-4).
- Frost, M.A., Goebel, R., 2012. Measuring structural–functional correspondence: spatial variability of specialised brain regions after macro-anatomical alignment. *Neuroimage* 59, 1369–1381. <https://doi.org/10.1016/j.neuroimage.2011.08.035>.
- Gabrieli, J.D., Ghosh, S.S., Whitfield-Gabrieli, S., 2015. Prediction as a humanitarian and pragmatic contribution from human cognitive neuroscience. *Neuron* 85, 11–26. <https://doi.org/10.1016/j.neuron.2014.10.047>.
- Gordon, E.M., Laumann, T.O., Adeyemo, B., Gilmore, A.W., Nelson, S.M., Dosenbach, N.U., Petersen, S.E., 2017a. Individual-specific features of brain systems identified with resting state functional correlations. *Neuroimage* 146, 918–939. <https://doi.org/10.1016/j.neuroimage.2016.08.032>.
- Gordon, E.M., Laumann, T.O., Adeyemo, B., Petersen, S.E., 2017b. Individual variability of the system-level organization of the human brain. *Cerebr. Cortex* 27, 386–399. <https://doi.org/10.1093/cercor/bhw239>.
- Greve, D.N., Fischl, B., 2009. Accurate and robust brain image alignment using boundary-based registration. *Neuroimage* 48, 63–72. <https://doi.org/10.1016/j.neuroimage.2009.06.060>.
- Guntupalli, J.S., Feilong, M., Haxby, J.V., 2018. A computational model of shared fine-scale structure in the human connectome. *PLoS Comput. Biol.* 14 (4) e1006120. <https://doi.org/10.1371/journal.pcbi.1006120>.
- Guntupalli, J.S., Hanke, M., Halchenko, Y.O., Connolly, A.C., Ramadge, P.J., Haxby, J.V., 2016. A model of representational spaces in human cortex. *Cerebr. Cortex* 26, 2919–2934. <https://doi.org/10.1093/cercor/bhw068>.
- Guntupalli, J.S., Wheeler, K.G., Gobbini, M.I., 2017. Disentangling the representation of identity from head view along the human face processing pathway. *Cerebr. Cortex* 27, 46–53. <https://doi.org/10.1093/cercor/bhw344>.
- Hackmack, K., Paul, F., Weygandt, M., Allefeld, C., Haynes, J.-D., 2012. Multi-scale classification of disease using structural MRI and wavelet transform. *Neuroimage* 62, 48–58. <https://doi.org/10.1016/j.neuroimage.2012.05.022>.
- Hanke, M., Halchenko, Y.O., Sederberg, P.B., Hanson, S.J., Haxby, J.V., Pollmann, S., 2009. PyMPPA: a python toolbox for multivariate pattern analysis of fMRI data. *Neuroinformatics* 7, 37–53. <https://doi.org/10.1007/s12021-008-9041-y>.
- Hasson, U., Nir, Y., Levy, I., Fuhrmann, G., Malach, R., 2004. Intersubject synchronization of cortical activity during natural vision. *Science* 303, 1634–1640. <https://doi.org/10.1126/science.1089506>.
- Haxby, J.V., Connolly, A.C., Guntupalli, J.S., 2014. Decoding neural representational spaces using multivariate pattern analysis. *Annu. Rev. Neurosci.* 37, 435–456. <https://doi.org/10.1146/annurev-neuro-062012-170325>.
- Haxby, J.V., Gobbini, M.I., Furey, M.L., Ishai, A., Schouten, J.L., Pietrini, P., 2001. Distributed and overlapping representations of faces and objects in ventral temporal cortex. *Science* 293, 2425–2430. <https://doi.org/10.1126/science.1063736>.
- Haxby, J.V., Guntupalli, J.S., Connolly, A.C., Halchenko, Y.O., Conroy, B.R., Gobbini, M.I., Hanke, M., Ramadge, P.J., 2011. A common, high-dimensional model of the representational space in human ventral temporal cortex. *Neuron* 72, 404–416. <https://doi.org/10.1016/j.neuron.2011.08.026>.
- Heuvel, M.P. van den, Stam, C.J., Kahn, R.S., Pol, H.E.H., 2009. Efficiency of functional brain networks and intellectual performance. *J. Neurosci.* 29, 7619–7624. <https://doi.org/10.1523/jneurosci.1443-09.2009>.
- Jenkinson, M., Bannister, P., Brady, M., Smith, S., 2002. Improved optimization for the robust and accurate linear registration and motion correction of brain images. *Neuroimage* 17, 825–841. <https://doi.org/10.1006/nimg.2002.1132>.
- Kanwisher, N., McDermott, J., Chun, M.M., 1997. The fusiform face area: a module in human extrastriate cortex specialized for face perception. *J. Neurosci.* 17, 4302–4311. <https://doi.org/10.1523/jneurosci.17-11-04302.1997>.
- Kriegeskorte, N., Goebel, R., Bandettini, P., 2006. Information-based functional brain mapping. *Proc. Natl. Acad. Sci. U.S.A.* 103, 3863–3868. <https://doi.org/10.1073/pnas.0600244103>.
- Kriegeskorte, N., Kievit, R.A., 2013. Representational geometry: integrating cognition, computation, and the brain. *Trends Cognit. Sci.* 17, 401–412. <https://doi.org/10.1016/j.tics.2013.06.007>.
- Kriegeskorte, N., Mur, M., Bandettini, P., 2008. Representational similarity analysis—connecting the branches of systems neuroscience. *Front. Syst. Neurosci.* 2, 4. <https://doi.org/10.3389/fnro.06.004.2008>.
- Misaki, M., Kim, Y., Bandettini, P.A., Kriegeskorte, N., 2010. Comparison of multivariate classifiers and response normalizations for pattern-information fMRI. *Neuroimage* 53, 103–118. <https://doi.org/10.1016/j.neuroimage.2010.05.051>.
- Nastase, S.A., Connolly, A.C., Oosterhof, N.N., Halchenko, Y.O., Guntupalli, J.S., Visconti di Oleggio Castello, M., Gors, J., Gobbini, M.I., Haxby, J.V., 2017. Attention selectively reshapes the geometry of distributed semantic representation. *Cerebr. Cortex* 27, 4277–4291. <https://doi.org/10.1093/cercor/bhx138>.
- Nieto-Castañón, A., Fedorenko, E., 2012. Subject-specific functional localizers increase sensitivity and functional resolution of multi-subject analyses. *Neuroimage* 63, 1646–1669. <https://doi.org/10.1016/j.neuroimage.2012.06.065>.
- Oosterhof, N.N., Wiestler, T., Downing, P.E., Diedrichsen, J., 2011. A comparison of volume-based and surface-based multi-voxel pattern analysis. *Neuroimage* 56, 593–600. <https://doi.org/10.1016/j.neuroimage.2010.04.270>.
- Petersson, K.M., Nichols, T.E., Poline, J.-B., Holmes, A.P., 1999. Statistical limitations in functional neuroimaging II. Signal detection and statistical inference. *Philos. Trans. R. Soc. B* 354, 1261–1281. <https://doi.org/10.1098/rstb.1999.0478>.
- Poldrack, R.A., 2017. Precision neuroscience: dense sampling of individual brains. *Neuron* 95, 727–729. <https://doi.org/10.1016/j.neuron.2017.08.002>.
- Power, J.D., Cohen, A.L., Nelson, S.M., Wig, G.S., Barnes, K.A., Church, J.A., Vogel, A.C., Laumann, T.O., Miezin, F.M., Schlaggar, B.L., Petersen, S.E., 2011. Functional network organization of the human brain. *Neuron* 72, 665–678. <https://doi.org/10.1016/j.neuron.2011.09.006>.
- Power, J.D., Mitra, A., Laumann, T.O., Snyder, A.Z., Schlaggar, B.L., Petersen, S.E., 2014. Methods to detect, characterize, and remove motion artifact in resting state fMRI. *Neuroimage* 84, 320–341. <https://doi.org/10.1016/j.neuroimage.2013.08.048>.
- Saxe, R., Brett, M., Kanwisher, N., 2006. Divide and conquer: a defense of functional localizers. *Neuroimage* 30, 1088–1096. <https://doi.org/10.1016/j.neuroimage.2005.12.062>.
- Sha, L., Haxby, J.V., Abdi, H., Guntupalli, J.S., Oosterhof, N.N., Halchenko, Y.O., Connolly, A.C., 2015. The animacy continuum in the human ventral vision pathway. *J. Cognit. Neurosci.* 27, 665–678. [https://doi.org/10.1162/jocn\\_a\\_00733](https://doi.org/10.1162/jocn_a_00733).
- Smith, S.M., Vidaurre, D., Beckmann, C.F., Glasser, M.F., Jenkinson, M., Miller, K.L., Nichols, T.E., Robinson, E.C., Salimi-Khorshidi, G., Woolrich, M.W., Barch, D.M., Ugurbil, K., Essen, D.C.V., 2013. Functional connectomics from resting-state fMRI. *Trends Cognit. Sci.* 17, 666–682. <https://doi.org/10.1016/j.tics.2013.09.016>.
- Spearman, C., 1904. The proof and measurement of association between two things. *Am. J. Psychol.* 15, 72–101. <http://psycnet.apa.org/doi/10.2307/1412159>.
- Tustison, N.J., Avants, B.B., Cook, P.A., Zheng, Y., Egan, A., Yushkevich, P.A., Gee, J.C., 2010. N4ITK: improved n3 bias correction. *IEEE Trans. Med. Imag.* 29, 1310–1320. <https://doi.org/10.1109/tmi.2010.2046908>.
- Vanderwal, T., Eilbott, J., Finn, E.S., Craddock, R.C., Turnbull, A., Castellanos, F.X., 2017. Individual differences in functional connectivity during naturalistic viewing conditions. *Neuroimage* 157, 521–530. <https://doi.org/10.1016/j.neuroimage.2017.06.027>.
- Van Horn, J.D., Grafton, S.T., Miller, M.B., 2008. Individual variability in brain activity: a nuisance or an opportunity? *Brain Imag. Behav.* 2, 327. <https://doi.org/10.1007/s11682-008-9049-9>.
- Visconti di Oleggio Castello, M., Halchenko, Y.O., Guntupalli, J.S., Gors, J.D., Gobbini, M.I., 2017. The neural representation of personally familiar and unfamiliar faces in the distributed system for face perception. *Sci. Rep.* 7. <https://doi.org/10.1038/s41598-017-12559-1>.
- Weiner, K.S., Barnett, M.A., Witthoft, N., Golarai, G., Stigliani, A., Kay, K.N., Gomez, J., Natu, V.S., Amunts, K., Zilles, K., Grill-Spector, K., 2018. Defining the most probable location of the parahippocampal place area using cortex-based alignment and cross-validation. *Neuroimage* 170, 373–384. <https://doi.org/10.1016/j.neuroimage.2017.04.040>.
- Weiner, K.S., Golarai, G., Caspers, J., Chuapoco, M.R., Mohlberg, H., Zilles, K., Amunts, K., Grill-Spector, K., 2014. The mid-fusiform sulcus: a landmark identifying both cytoarchitectonic and functional divisions of human ventral temporal cortex. *Neuroimage* 84, 453–465. <https://doi.org/10.1016/j.neuroimage.2013.08.068>.
- Wolfers, T., Buitelaar, J.K., Beckmann, C.F., Franke, B., Marquand, A.F., 2015. From estimating activation locality to predicting disorder: a review of pattern recognition for neuroimaging-based psychiatric diagnostics. *Neurosci. Biobehav. Rev.* 57, 328–349. <https://doi.org/10.1016/j.neubiorev.2015.08.001>.
- Woo, C.-W., Chang, L.J., Lindquist, M.A., Wager, T.D., 2017. Building better biomarkers: brain models in translational neuroimaging. *Nat. Neurosci.* 20, 365–377. <https://doi.org/10.1038/nn.4478>.
- Yamada, K., Miyawaki, Y., Kamitani, Y., 2015. Inter-subject neural code converter for visual image representation. *Neuroimage* 113, 289–297. <https://doi.org/10.1016/j.neuroimage.2015.03.059>.
- Yeo, B.T.T., Krienen, F.M., Sepulcre, J., Sabuncu, M.R., Lashkari, D., Hollinshead, M., Roffman, J.L., Smoller, J.W., Zöllei, L., Polimeni, J.R., Fischl, B., Liu, H., Buckner, R.L., 2011. The organization of the human cerebral cortex estimated by intrinsic functional connectivity. *J. Neurophysiol.* 106, 1125–1165. <https://doi.org/10.1152/jn.00338.2011>.
- Zhen, Z., Kong, X.-Z., Huang, L., Yang, Z., Wang, X., Hao, X., Huang, T., Song, Y., Liu, J., 2017. Quantifying the variability of scene-selective regions: interindividual, interhemispheric, and sex differences. *Hum. Brain Mapp.* 38, 2260–2275. <https://doi.org/10.1002/hbm.23519>.
- Zhen, Z., Yang, Z., Huang, L., Kong, X.-z., Wang, X., Dang, X., Huang, Y., Song, Y., Liu, J., 2015. Quantifying interindividual variability and asymmetry of face-selective regions: a probabilistic functional atlas. *Neuroimage* 113, 13–25. <https://doi.org/10.1016/j.neuroimage.2015.03.010>.
- Zhou, Z.-H., 2012. *Ensemble Methods: Foundations and Algorithms*. Chapman & Hall/CRC, Boca Raton, FL.